energies

MDPI

Article

Numerical and Experimental Analysis of Shell and Tube Heat Exchanger with Round and Hexagonal Tubes

Abdullah Khan [1], Imran Shah [2,*], Waheed Gul [1], Tariq Amin Khan [2], Yasir Ali [2] and Syed Athar Masood [3]

[1] Department of Mechanical Engineering, National University of Technology, Islamabad 44000, Pakistan
[2] Department of Aerospace Engineering, College of Aeronautical Engineering, National University of Sciences and Technology, Risalpur 24090, Pakistan
[3] Department of Mechanical Engineering, International Islamic University, Islamabad 44000, Pakistan
* Correspondence: imranshahswabi@gmail.com

Abstract: Shell and tube heat exchangers are used to transfer thermal energy from one medium to another for regulating fluid temperatures in the processing and pasteurizing industries. Enhancement of a heat transfer rate is desired to maximize the energy efficiency of the shell and tube heat exchangers. In this research work, we performed computational fluid dynamics (CFD) simulations and experimental analysis on the shell and tube heat exchangers using round and hexagonal tubes for a range of flow velocities using both parallel flow and counter flow arrangements. In the present work, the rate of heat transfer, temperature drop, and heat transfer coefficient are computed using three turbulence models: the Spalart–Allmaras, the k-epsilon (RNG), and the k-omega shear stress transport (SST). We further utilized the logarithmic mean temperature difference (LMTD) method to compute the heat transfer and mass flow rates for both parallel and counter flow arrangements. Our results show that the rate of heat transfer is increased by introducing the hexagonal structure tubes, since it has better flow disruption as compared to the round tubes. We further validated our simulation results with experiments. For more accurate results, CFD is performed in counter and parallel flow and it is deduced that the rate of heat transfer directly depends upon the velocity of fluids and the number of turns of the tube.

Keywords: shell and tube heat exchanger; computational fluid dynamics; hexagonal tubes; Ansys Fluent; temperature drop; Reynolds number

Citation: Khan, A.; Shah, I.; Gul, W.; Khan, T.A.; Ali, Y.; Masood, S.A. Numerical and Experimental Analysis of Shell and Tube Heat Exchanger with Round and Hexagonal Tubes. *Energies* **2023**, *16*, 880. https://doi.org/10.3390/en16020880

Academic Editors: Xinyu Wang, Jingzhi Zhang and Gongming Xin

Received: 11 December 2022
Revised: 5 January 2023
Accepted: 10 January 2023
Published: 12 January 2023

1. Introduction

Heat exchangers are devices used for transferring thermal energy between a solid object and a fluid, or between two or more fluids with an existing temperature difference [1]. Synthetic process industries, such as power generation, petrochemical, and heat recovery systems, employ heat exchangers as a means of supplying effective and suitable heat conduction for heating, cooling, and material phase change. Shell and tube heat exchangers are comprised of a shell (a large pressure vessel) with a batch of tubes centered in it [2]. The efficiency of shell and tube heat exchangers depends upon the geometry of tubes since it determines the rate of heat transfer between the fluids at different temperatures. The geometry of these tubes affects the heat transfer rate between the fluids by varying the surface area exposed for heat transfer [3].

The exchange of thermal energy between the fluids at different temperatures occurs across the tubes [4]. The heat transfer rate directly depends upon the geometry of tubes and the velocity of a fluid floating inside it [5]. Researchers have tried to maximize the heat transfer rate by optimizing the blade geometry [6,7]. Introducing the hexagonal tubes inside the shell of a heat exchanger increases the exposed surface for heat transfer and maximizes the surface area [8]. Hexagonal tubes have six-face geometry that enhances the fluid mixing, due to which the heat transfer coefficient is maximized.

CFD analysis assists in analyzing the characteristics of a heat exchanger [9,10]. The flow around and within the tubes of a heat exchanger is very complex and sophisticated equipment is needed to capture the visual effects. [11]. Therefore, CFD analysis allows for the observation of flow characteristics at the inaccessible locations of the shell and tube heat exchangers. Multiple CFD techniques are used to simulate the flow inside the tubular heat exchanger [12]. These techniques are actuator lines, actuator disks, and fully resolved rotors [13].

The round tube heater exchanger deteriorates due to environmental fouling. Oxidations and hot corrosions cause the round tubes to corrode with time. In comparison, the hexagonal tubes reduce corrosion by distributing the gradients of fouling over its surface. The hexagonal tubes maximize the surface area, which reduces the risk of damage [14].

Many efforts are made to study the flow and heat transfer characteristics of shell and tube heat exchangers. Gurbir Singh et al. [15] present the CFD analysis of a single shell and tube-type heat exchanger and compare the results with the experimental data. Chuncula Babu et al. [16] studied the different passive techniques that can be applied in the tube of a heat exchanger. Ram Kishan et al. [17] numerically investigated the different flow patterns in the tubes of a shell and tube heat exchanger. Sharma et al. [18] examined the flow patterns, pressure drop, and heat transfer coefficient in staggered and inline shell-tube heat exchangers. Kumar et al. [19] studied the heat and flow characteristics of the double helically coiled tube heat exchanger. However, research is lacking in the investigation of tubes in a turbulent flow regime. Furthermore, research is needed to improve the efficiency of heat exchangers by optimizing the tube geometry [20].

In this research work, we increased the efficiency of the heat exchanger by introducing hexagonal tubes instead of round tubes. We studied the effect of design modifications on the efficiency of the heat exchanger. Numerical and experimental examination of the heat and flow characteristics at multiple fluid velocities are carried out and the number of turns in tubes is optimized to enhance the efficiency. Introducing the hexagonal geometry for the tubes of a heat exchanger increases the rate of heat transfer because its increases in surface area for heat transfer and flow dynamics is varied. The numerical and experimental results were conducted at various fluid velocities, ranging from 0.75 m/s to 2.75 m/s along with the multiple numbers of turns in the tubes.

2. Physical Model

Shell and tube heat exchangers are comprised of a shell with a bundle of inner tubes where heat transfer occurs [21–24]. These tubes have multiple numbers of turns that enhance the heat transfer rate. In this research work, a shell and tube heat exchanger is designed in the SOLIDWORKS as shown in Figure 1. A detailed description of all of the individual components is given in the Supplementary File where the end caps, shell, tubes, and stand are shown in Figure S1. Table 1 depicts the parameters of the heat exchanger.

Table 1. Design parameters of the heat exchanger.

Sr. No	Parameter	Value
1	Tube Diameter	30 mm
2	Shell Diameter	180 mm
3	Number of Tubes	9
4	Overall Length	500 mm
5	Tube Thickness	2.5 mm
6	Shell Thickness	2.0 mm
7	Number of Turns	3 to 14

Table 2 shows the geometric and flow parameters. The geometries of the round and hexagonal tube bundles with baffles are shown in Figure 2a,b, respectively, and the cross-section view of the tubes are represented in Figure 2c. The tubes' lengths and thicknesses are kept the same for both designs, at 120 mm and 2.5 mm, respectively. The number

of tapping points is 59 for both tubes. The surface area of round and hexagonal tubes is 723 mm^2 and 976 mm^2, respectively. Table 3 shows the material properties [25,26].

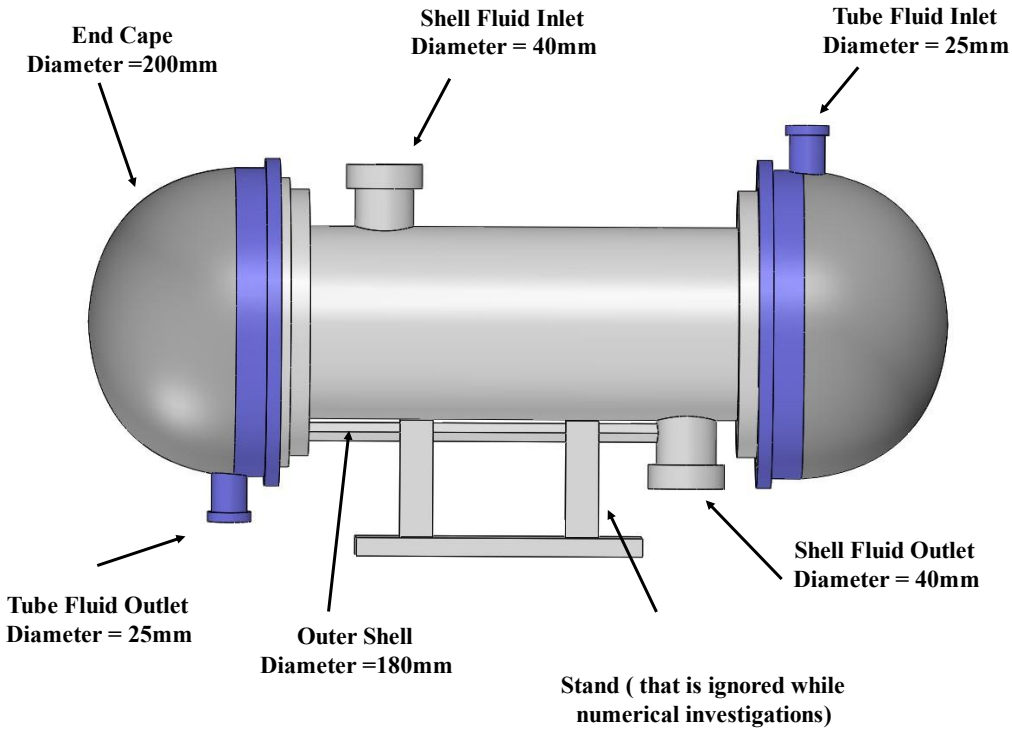

Figure 1. CAD Design of the Shell and Tube Heat Exchanger.

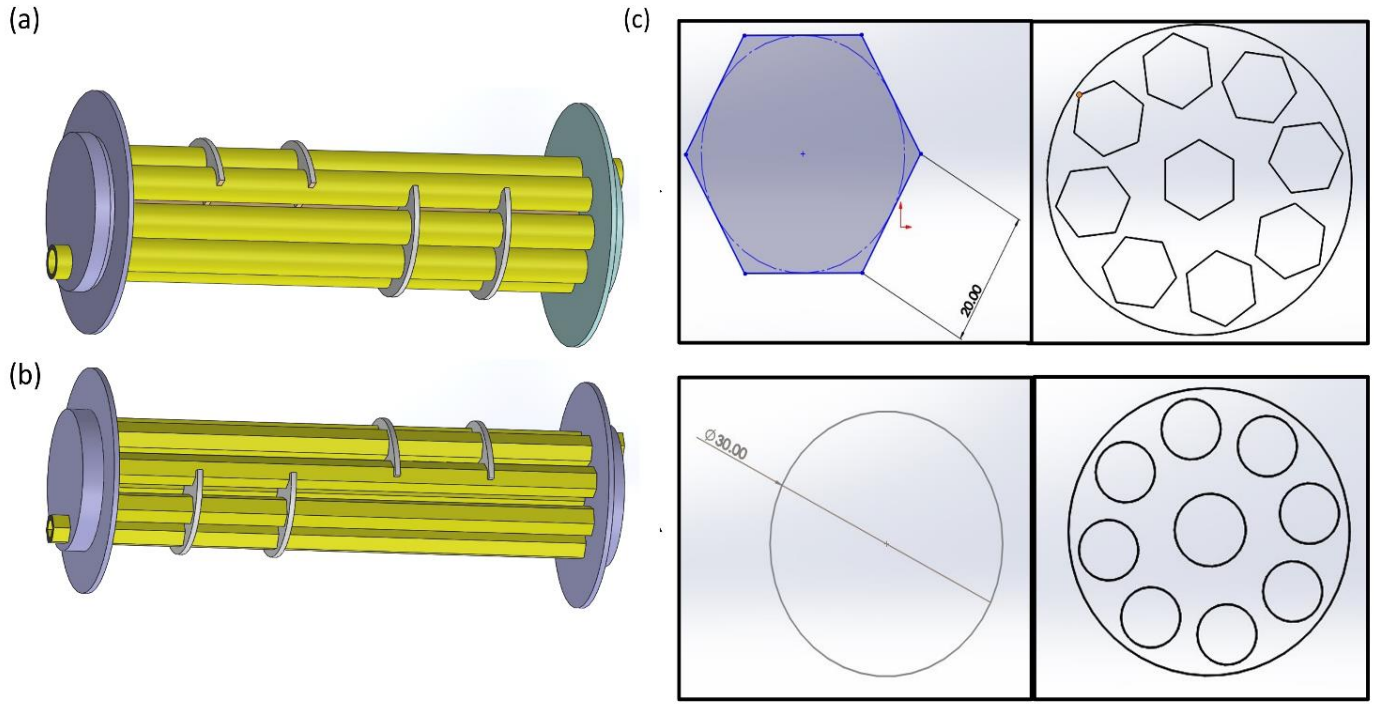

Figure 2. (**a**) Round tubes heat exchanger; (**b**) designed hexagonal tubes heat exchanger; (**c**) cross-sectional view of tubes for hexagonal and round shapes.

Table 2. Conditions of Round Tubes Heat Exchanger.

Geometry	Fluid Velocity (m/s)	Number of Turns	Tubes Length (mm)	Number of Baffles	Tapping Points	Surface Area (mm^2)
Round tube Geometry	0.75 to 2.75	03 to 14	320	04	59	723
Hexagonal Geometry	0.75 to 2.75	03 to 14	320	04	59	976

Table 3. Properties of the selected materials used in numerical simulations.

Part	Material	Poison Ratio	Yield Strength	Thermal Conductivity
Tubes	Copper	0.314	33 MPa	398 W/m·K
Shell	Aluminum	0.32	276 MPa	251 W/m·K
End Caps	Mild Steel	0.3	250 MPa	45 W/m·K

2.1. Numerical Methodology

The mathematical equations used in the analysis of heat and flow characteristics are given below. The rate of heat transfer between the fluids at different temperatures is computed using the following equation:

$$Q^{\circ} = UA_S\Delta T_{lm} \tag{1}$$

where U is the heat transfer coefficient. The surface area is computed in the SOLIDWORKS as shown in Figure S2. The logarithmic mean temperature difference is calculated using the following equation [27–29]:

$$\Delta T_{lm} = \frac{\Delta T_1 - \Delta T_2}{In\ \Delta T_1 - In\ \Delta T_2} \tag{2}$$

The initial and final temperature differences depend on the nature of the flow of the fluid. Temperature differences for the parallel flow and the counter flow are described briefly in the following equations:

- Parallel flow

  - $\Delta T_1 = T_{hi} - T_{ci}$
  - $\Delta T_2 = T_{ho} - T_{co}$

- Counterflow

  - $\Delta T_1 = T_{hi} - T_{co}$
  - $\Delta T_2 = T_{ho} - T_{ci}$

1. $T_{hi} = Hot\ inlet\ temperature$
2. $T_{ho} = Hot\ outlet\ temperature$
3. $T_{ci} = Cold\ inlet\ temperature$
4. $T_{co} = Cold\ outlet\ temperature$

The governing equations of the flow are modified according to the conditions. In this case, the problem is assumed to be a steady state. Therefore, all the time-dependent parameters are omitted from the governing equations [28,29].

$$\text{Conservation of the mass } \frac{\partial p}{\partial t} + \nabla.(pv) = 0 \tag{3}$$

$$\text{X momentum equation } \nabla.(puV) = -\frac{\partial p}{\partial x} + \frac{\partial \tau_{xx}}{\partial x} + \frac{\partial \tau_{yx}}{\partial y} + \frac{\partial \tau_{zx}}{\partial z} \tag{4}$$

$$\text{Y momentum equation } \nabla.(puV) = -\frac{\partial p}{\partial y} + \frac{\partial \tau_{xy}}{\partial x} + \frac{\partial \tau_{yy}}{\partial y} + \frac{\partial \tau_{zy}}{\partial z} + pg \quad (5)$$

$$\text{Z momentum equation } \nabla.(puV) = -\frac{\partial p}{\partial y} + \frac{\partial \tau_{xz}}{\partial x} + \frac{\partial \tau_{yz}}{\partial y} + \frac{\partial \tau_{zz}}{\partial z} \quad (6)$$

$$\text{Energy } \nabla.(peV) = -p\nabla.V + \nabla.(k\nabla T) + q + \Phi \quad (7)$$

$$\Phi = \mu\left[2[\left(\frac{\partial u}{\partial x}\right)^2 + \left(\frac{\partial v}{\partial y}\right)^2 + \left(\frac{\partial w}{\partial z}\right)^2\right] + \left(\frac{\partial u}{\partial y} + \frac{\partial v}{\partial x}\right)^2 \left(\frac{\partial u}{\partial z} + \frac{\partial w}{\partial x}\right)^2 + \left(\frac{\partial v}{\partial z} + \frac{\partial w}{\partial y}\right)^2] + \lambda(\nabla.V)^2 \quad (8)$$

Turbulence modeling is done to cater for the turbulence effects. The Spalart–Allmaras, k-omega SST, and k-epsilon RNG models are considered in this study. The model is solved using Ansys Fluent software with a Finite volume approach. Upwind-based multidimensional linear approach and upwind discretization schemes are utilized in the solver.

All the numerical simulations are performed with the same conditions adopted in the experiments. The air inlet velocity ranges from 0.75 m/s to 2.75 m/s at a Reynolds number from 10,000 to 15,000, whereas the outlet is at an ambient atmospheric condition. The 16.0 unstructured grid is considered with the sphere influence perspective adopted to congeal the grid around the model. The surface is termed as the boundaries that are at the left, right, bottom, top, and rears, up to 10D, 10D, 10D, 10D, and 15D, respectively, from the surface of a model, where D is the radius of the downstream. Mesh diagrams of cross-sections of round and hexagonal tubes are shown in the Figure S3 of the attached Supplementary File.

Figure 3a shows the computational domain, which is comprised of inlets and outlets for hot and cold fluid. The remaining boundaries are the walls and symmetry at which the symmetric tubes are placed. Hot fluid and cold fluid enter the computational domain at the temperature of 353 K and 300 K, respectively. Figure 3b shows the grid independence test for heat rate at different mesh sizes. In numerical simulations, the pressure coefficient for the finer mesh differs in relation to the coarse mesh by 0.54%, which is compatible with the dependency test. After the mesh independence test, the results are obtained from mesh which contained 2,143,020 elements and 2,871,035 nodes. After meshing the tube, again the shell meshing is done. Again, the boundary layer is created on the outside edge of the tube to mesh the face near the wall of the tube. Figure 3c shows the mesh sample along with magnified views for the hexagonal tube heat exchanger.

In the numerical analysis, the flow is considered as steady and incompressible. The fluid enters into the computational domain at a velocity ranging from 0.75 m/s to 2.75 m/s at a Reynolds number of 10,000 to 15,000. The density of water is 997 kg/m^3, whereas the viscosity of water is 1.78 $\times$ 10^{-5} kg/m.s [30].

2.2. Experimental Investigation

An actual model of the heat exchanger is fabricated and the setup is developed to perform the experimental investigation. Figure 4 depicts the schematic diagram of the fabricated model of the heat exchanger. Major operations that are performed for its fabrication are drilling welding, forging, and vacuum pressing, whereas its major components are outer shell, copper tubes (round and hexagonal), end caps, stand, pipes, and temperature sensors. The detail of the fabrication of the outer shell, end caps, and plates are shown in Figure S4, whereas the adjustable fluid pump and temperature sensors are shown in Figure S5. Figure S6 depicts the bending and the joining of the round-shaped tubes that are congregated in the shell of the heat exchanger. Details of the instrument used in the experimental computation are determined in Table S1 of the attached Supplementary File.

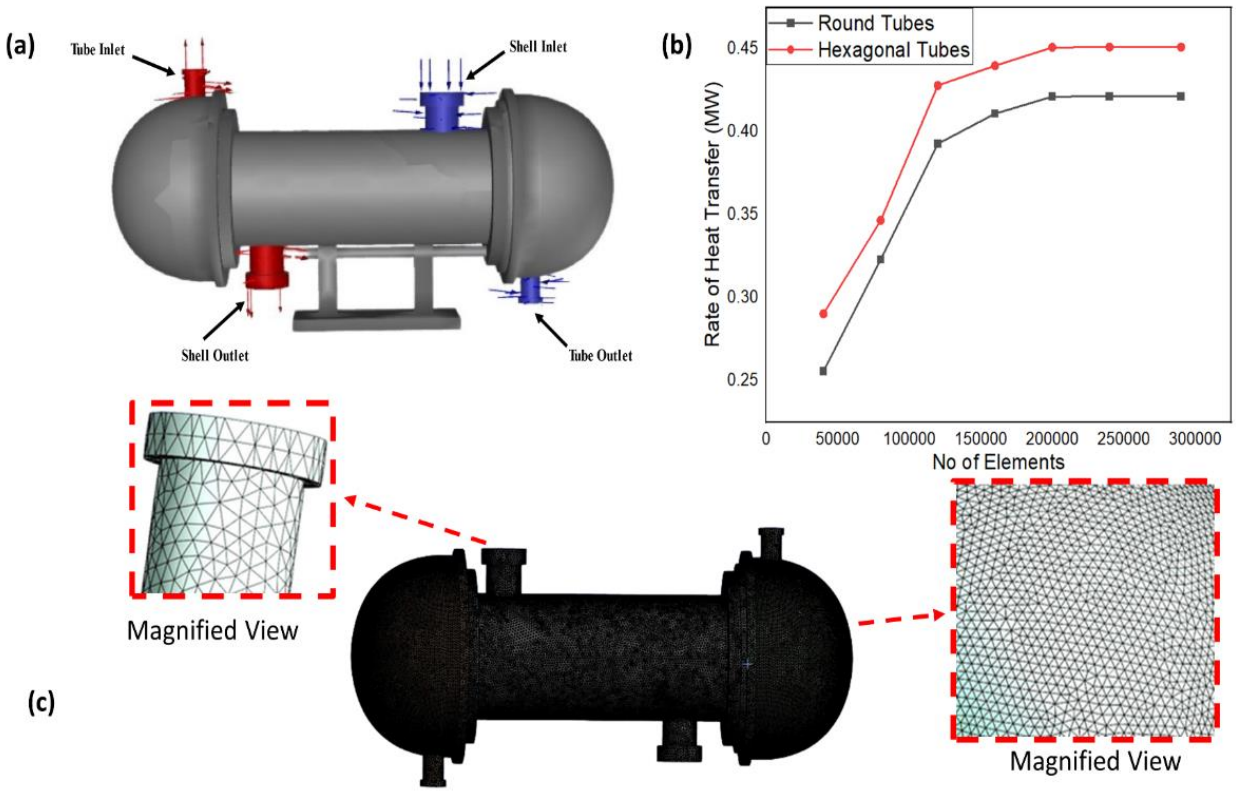

Figure 3. (**a**) Computational domain showing the inlets and outlets for shell and tube fluids; (**b**) mesh independence rest line plot; (**c**) meshing sample along with magnified views.

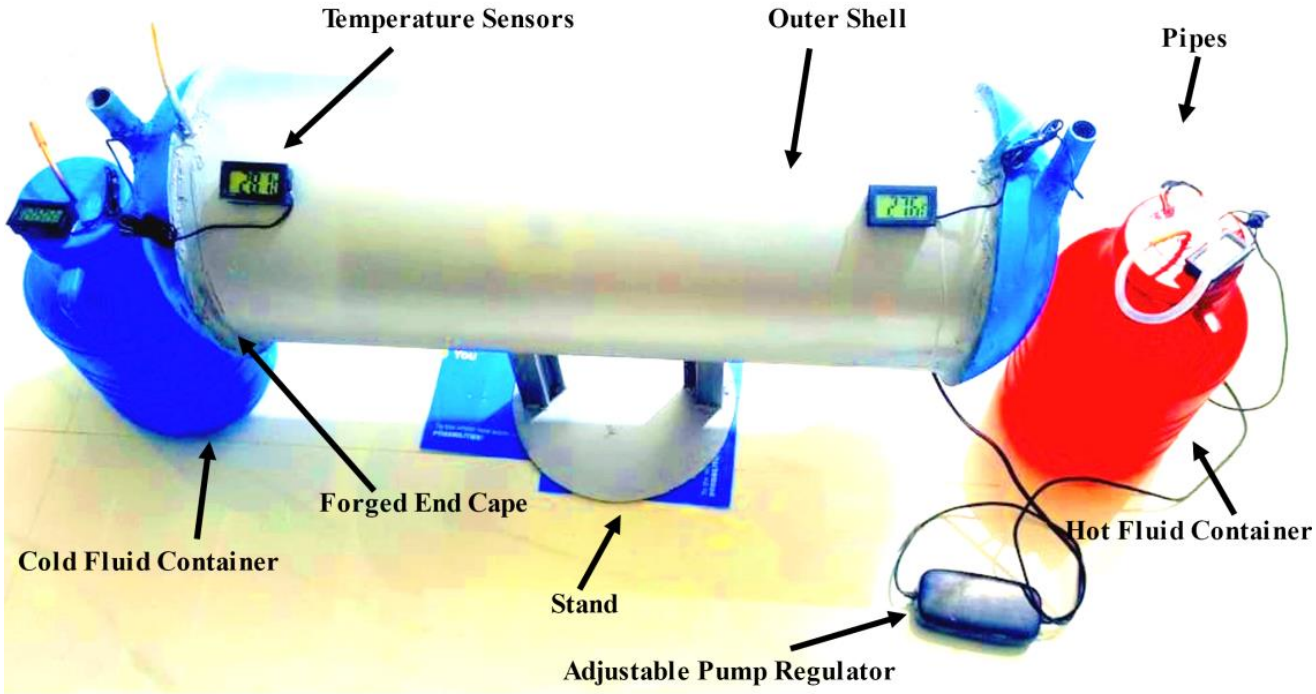

Figure 4. Schematic diagram of the fabricated model of the heat exchanger.

2.3. Experimental Computation

Water is used as the working fluid for both hot and cold fluid streams. The hot-water loop and cold-water loop are connected separately to the heat exchanger. Experiments are performed with the round and hexagonal tubes in which the hot fluid from the red

tank enters into the heat exchanger and cool fluid enters the blue tank after passing from the tubes.

3. Result and Discussion

Numerical and experimental examinations are performed on both the round and hexagonal tube heat exchangers at a Reynolds number from 10,000 to 15,000.

3.1. Heat Transfer Curve

Figure 5 depicts the rate of numerical heat transfer for hexagonal and round tube heat exchangers at parallel and counter flow at various fluid velocities. The heat transfer rate is increased by increasing the fluid velocity since more heat transfer occurs in the hexagonal tube heat exchanger as compared to the round tube heat exchanger. By enhancing the fluid velocity, the heat transfer enhances due to an increase in the proportion of eddies that rises as the overall heat transfer coefficient rises. Figure 5b indicates that heat transfer occurs in the counter flow heat exchanger as compared to the parallel flow heat exchanger because thermal energy distributes more evenly due to accelerated fluid flow in a counter flow heat exchanger.

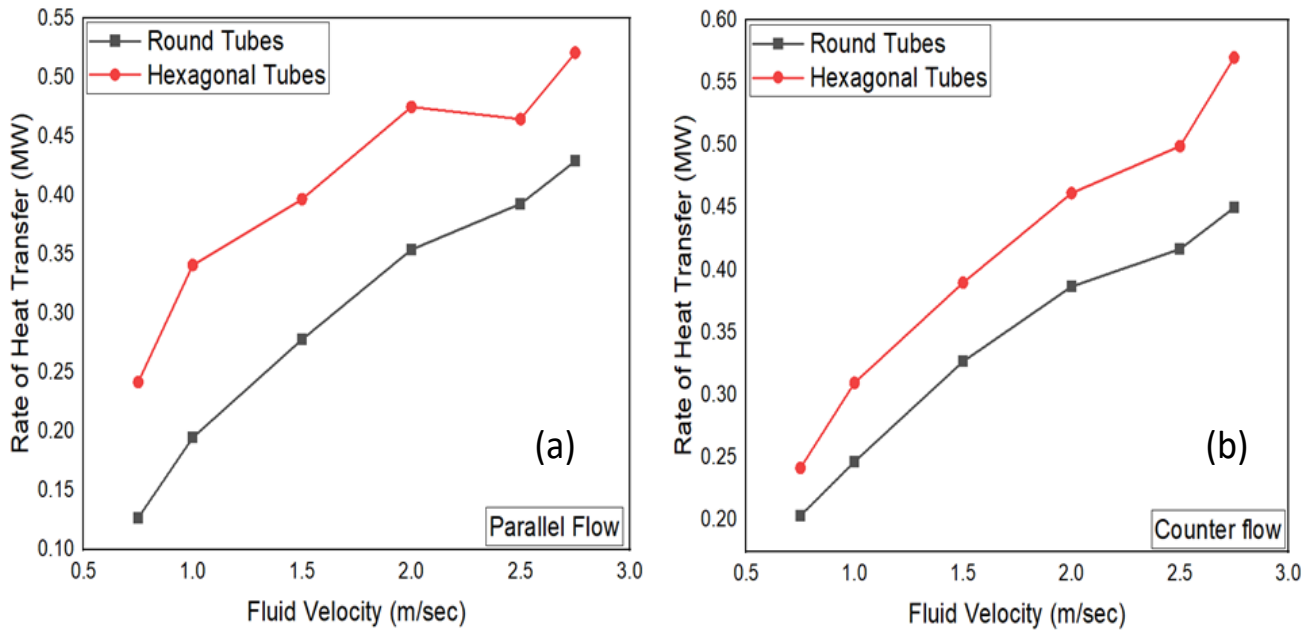

Figure 5. (**a**) Variation of the heat transfer rate due to fluid velocity in parallel flow; (**b**) variation of the heat transfer rate due to fluid velocity in counter flow.

Figure 6 depicts the numerical heat transfer rate for hexagonal and round tube heat exchangers at parallel and counter flow at various numbers of turns of tubes. The heat transfer rate increases by increasing the number of turns of a tube; however, colossal heat exchanges are seen in the case of hexagonal tubes as compared to the round circular tubes. By increasing the number of turns of a tube, the heat transfer enhances due to an increase of fluctuations that enhance the turbulence to the boundary layers. Figure 6b indicates that the magnitude of enhancement of the heat transfer rate is more pronounced in a counter flow heat exchanger as compared to a parallel flow heat exchanger. This is because in a counter flow heat exchanger, the thermal energy distributes more evenly due to accelerated fluid flow.

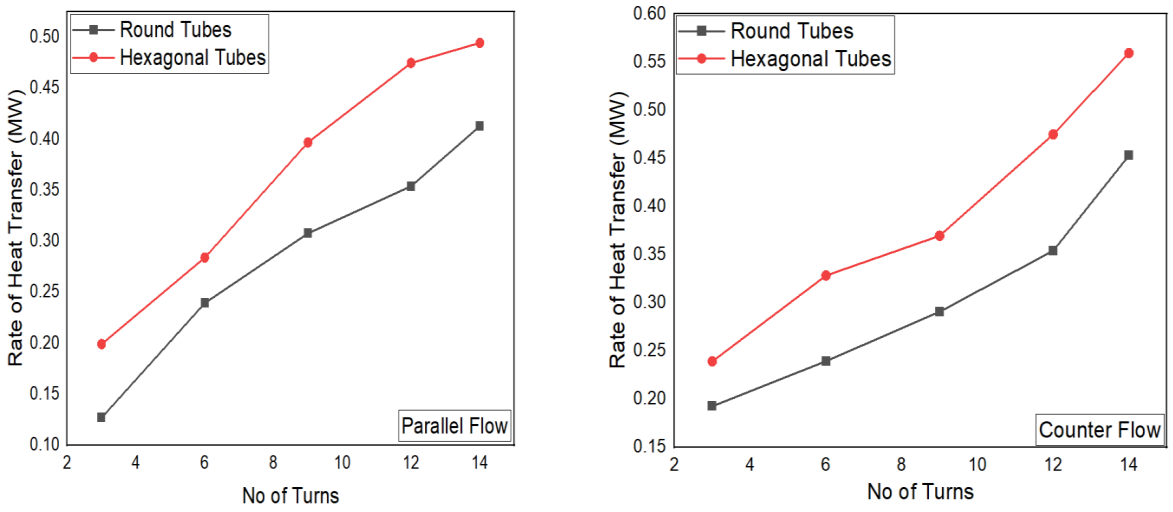

Figure 6. (**a**) Variation of the heat transfer rate due to the number of turns of the tube in (**a**) parallel flow; (**b**) in counter flow.

3.2. Pressure and Temperature Contours

Figure 7 shows the numerical pressure contours of a round (a) and hexagonal tube (b) heat exchanger, respectively. Figure 8 depicts the pressure drop at cross-sections of (a) round and (b) hexagonal tubes of heat exchanger at 100 mm, 250 mm, and 450 mm. It can be observed that due to higher flow disruption, the pressure drop is higher for the heat exchanger with hexagonal tubes compared to round tubes. Figure 8a shows the temperature contours that flow over round (a) and hexagonal tube (b) heat exchangers, respectively, whereas Figure 8b depicts the temperature contours at different cross-sections of the two types of tubes in the heat exchangers.

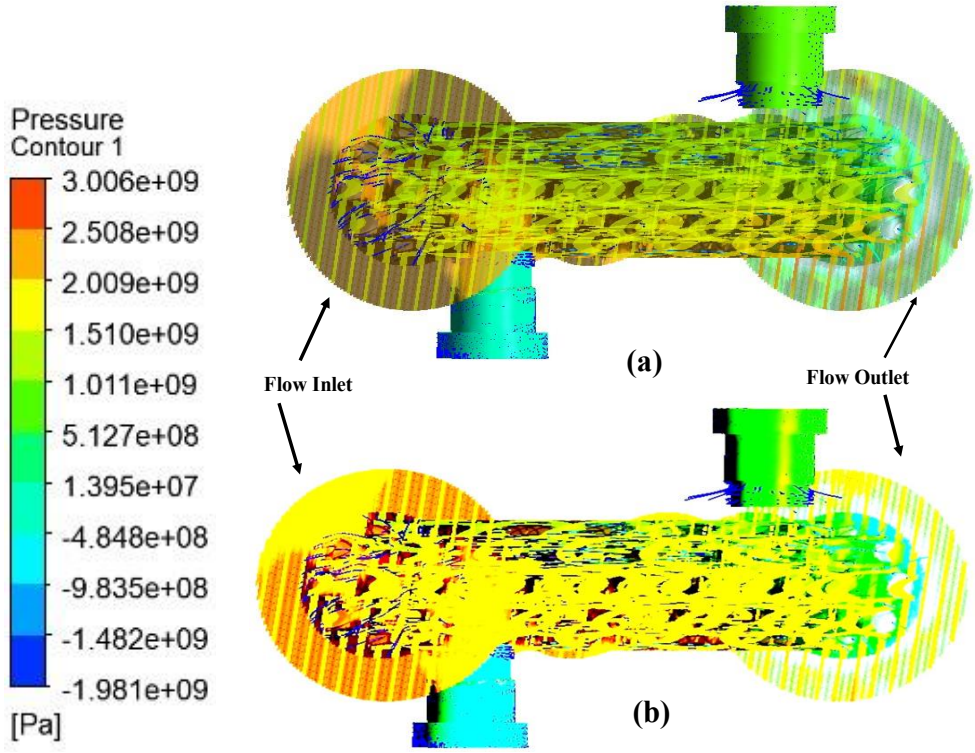

Figure 7. Pressure contours of (**a**) round tubes and (**b**) hexagonal tubes of a heat exchanger.

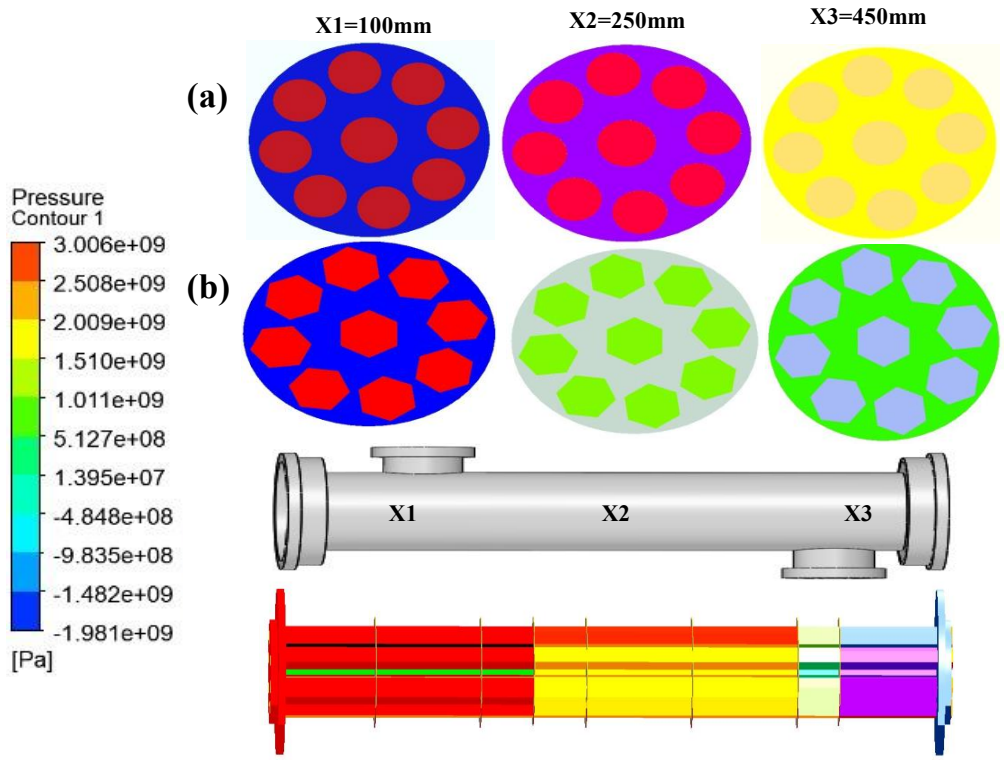

Figure 8. Pressure contours at cross-sections of (**a**) round tubes and (**b**) hexagonal tubes of a heat exchanger at 100 mm, 250 mm, and 450 mm.

Hexagonal tubes enhance the heat transfer of a heat exchanger by increasing the pressure drop of a fluid, as depicted in Figure 9. By increasing the pressure drop, the steady volume flow rate increases because of an increase in the density difference in a loop that acts as a driving force for heat to consign between the fluids. Hexagonal tubes increase the pressure drop of fluid, thus increasing its temperature, according to Gay Lussac's Law, thus increasing the heat transfer rate. The rate of heat transfer directly depends upon the surface area of tubes because the geometry of the tube determines the contact surface tubes and shell fluids. Hexagonal tubes enhance the heat transfer by escalating the surface area of the tubes due to which the proportion of the molecules conducting heat increases, thus increasing the heat transfer rate by increasing the temperature difference, as shown in Figure 10. Convergences of a heat transfer for round and hexagonal geometries, respectively, of the fully developed flow are shown in Figure 11.

Figure 11 depicts that at a minor number of iterations when the flow is developing the magnitude of the heat transfer rate are alternating continuously; however, when the flow is developed completely it becomes anchored. Hexagonal tubes distribute the thermal energy in its six-face geometry in such a way that even when a flow is developing, the rate of heat transfer is more pronounced than in round circular geometry. The heat transfer rate for round and hexagonal geometries at optimum fluid velocity is determined in Table 4.

Table 4. CFD heat transfer rates are computed at the optimum fluid velocity.

Round Tubes	Hexagonal Tubes
$Q^{\circ} = 0.325\ M\ W$	$Q^{\circ} = 0.514\ M\ W$

Table 5 shows the computation of the heat transfer rate in both the geometries of the tubes by LMTD. Hexagonal tubes signify the surface area and overall heat transfer coefficient that increases the heat transfer rate.

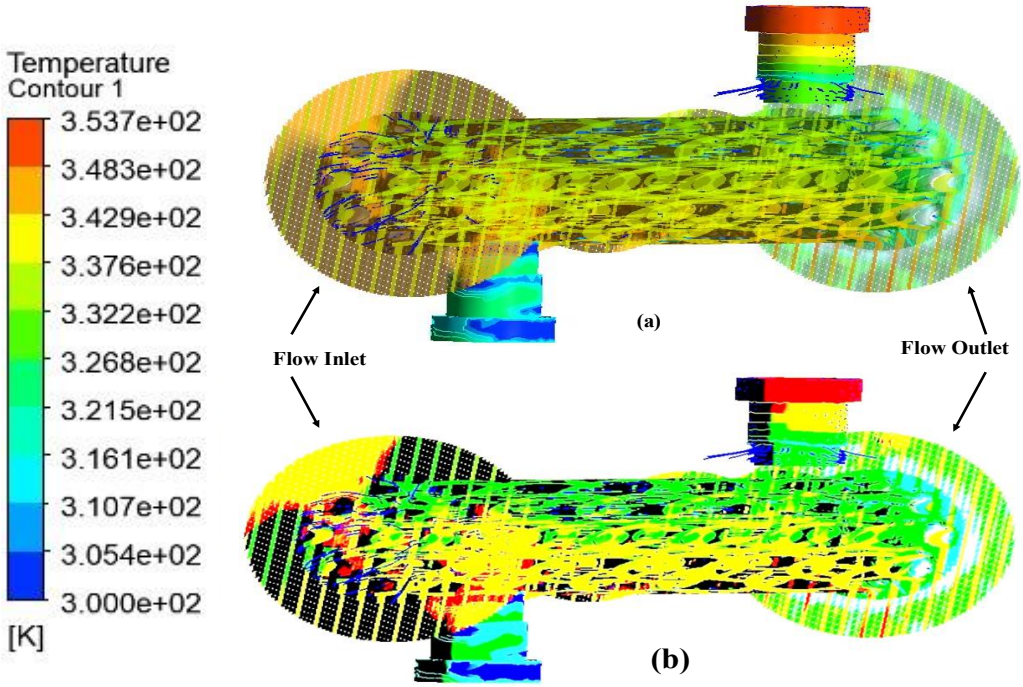

Figure 9. Temperature contours of (**a**) round tubes and of (**b**) hexagonal tubes of a heat exchanger.

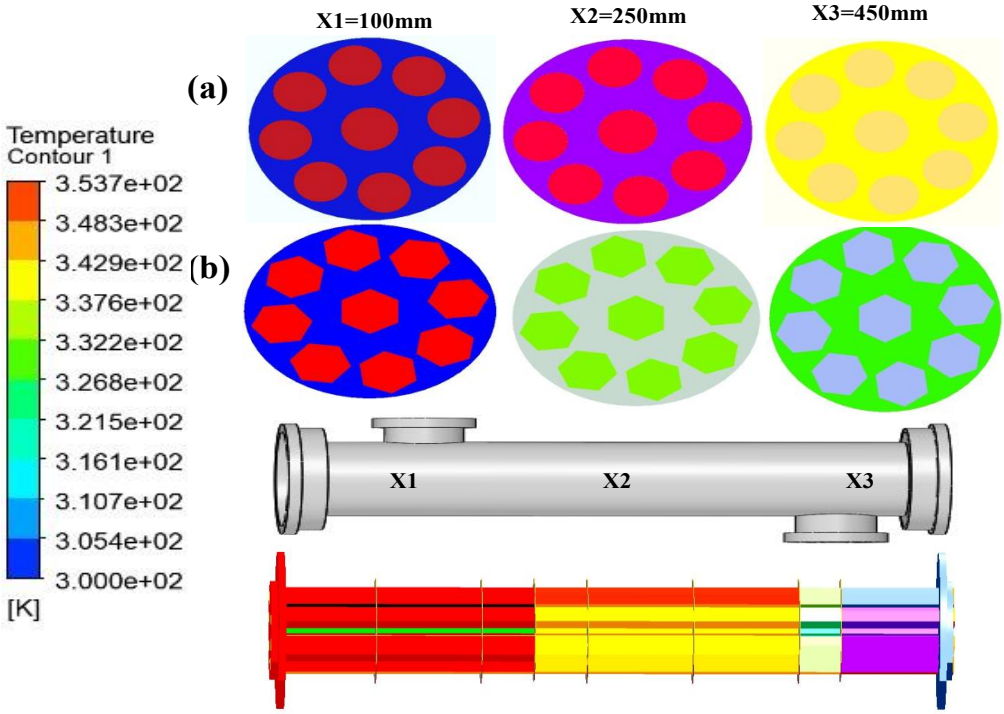

Figure 10. Temperature contours at cross-sections of (**a**) round tubes and (**b**) hexagonal tubes of a heat exchanger at 100 mm, 250 mm, and 450 mm.

The above numerical and experimental results show that the capability of a heat exchanger can be enhanced by introducing the hexagonal geometry on its tubes. Hexagonal geometry increases the surface area of the tubes, due to which the proportion of the molecules conducting heat is increased. The hexagonal geometry tubes increase the pressure drop of a fluid, due to which the steady mass flow rate increases because of the density differences. A number of experiments conclude that the effect of fluid velocity and the number of turns of tubes on the heat transfer rate is more pronounced in the

counter flow heat exchanger because the temperature is distributed more uniformly in the counter flow arrangement. The fluid velocity is adjusted numerically and experimentally and it is found that the maximum efficiency of tubes is accomplished at 2.57 m/s. The optimum velocity for fluid flow in the tubes of the heat exchanger is 2.57 m/s because the paramount heat transfer occurs at this fluid velocity. The results have uncertainty due to the following reasons.

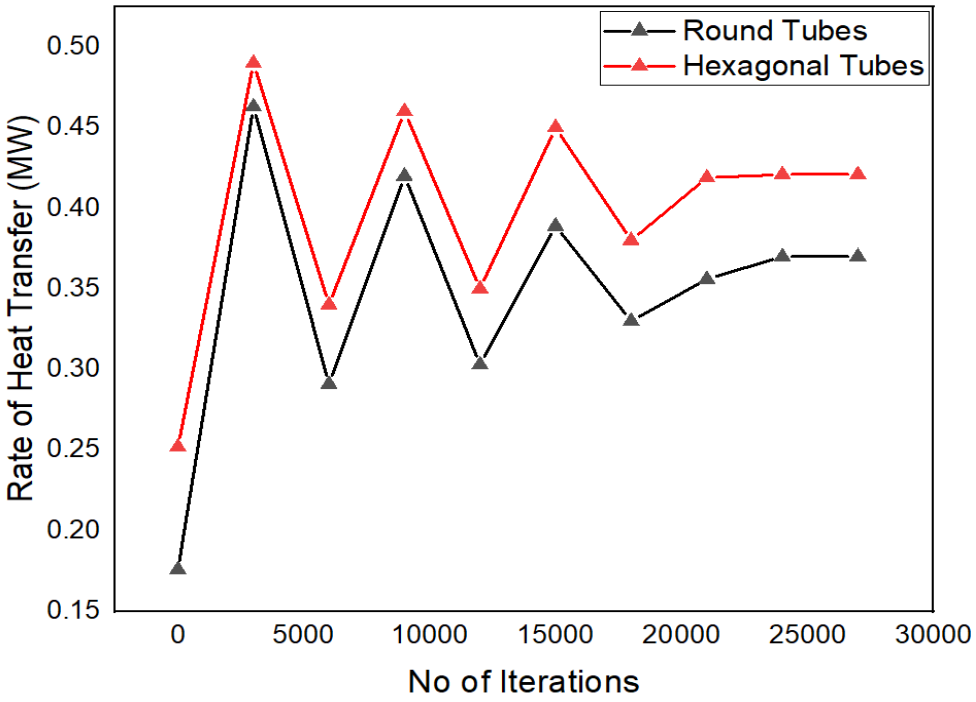

Figure 11. Heat transfer convergence plot.

Table 5. Computation of the experimental heat transfer rates at fluid velocity.

Round Tubes	Hexagonal Tubes
Rate of heat transfer $(Q^{\circ}) = UA_S\Delta T_{lm}$	Rate of heat transfer $(Q^{\circ}) = UA_S\Delta T_{lm}$
U = 640 Wm^{-2}/K	U = 665 Wm^{-2}/K
A_s = 7.12 m^2	A_s = 9.71 m^2
ΔT_1 = 75 Degrees Celsius	ΔT_1 = 80 Degrees Celsius
ΔT_2 = 82 Degrees Celsius	ΔT_2 = 100 Degrees Celsius
$\Delta T_{lm} = \frac{75-90}{In\,75-In\,90}$	$\Delta T_{lm} = \frac{80-100}{In\,80-In\,100}$
ΔT_{lm} = 82 Degrees Celsius	ΔT_{lm} = 90 Degrees Celsius
$Q^{\circ} = 640 \times 7.12 \times 82$	$Q^{\circ} = 665 \times 9.71 \times 90$
$Q^{\circ} = 373,657\ W$	$Q^{\circ} = 581,143\ W$

Table 6 presents the uncertainty calculation of both round and hexagonal tube heat exchangers and the distinction between the constant boundary conditions in CFD and the actual (variable) boundary conditions in the experiments. These boundary conditions are supposed to be continuous in CFD and the experiments. The physical model of the heat exchanger may have some functional errors that cause the distinction between the Q° (EXP) and Q° (CFD). The heat exchanger tubes may have blockage effects at the inlet or exit that cause the difference between the experimental and CFD coefficients.

The comparison of the results with some other research is shown in Table 7.

Table 6. Uncertainty calculation on both the tubes of a heat exchanger at optimum fluid velocity.

Round Tubes	Hexagonal Tubes
CFD	**CFD**
$Q^{\circ} = 0.325\ M\ W$	$Q^{\circ} = 0.514\ M\ W$
Experimental	**Experimental**
$Q^{\circ} = 0.37\ M\ W$	$Q^{\circ} = 0.559\ M\ W$
Uncertainty	**Uncertainty**
Rate of heat transfer Uncertainty = $(0.354 - 0.325)/0.325 = 9.2\%$	Rate of heat transfer Uncertainty = $(0.535 - 0.515)/0.525 = 4.1\%$

Table 7. Comparison of results.

Sr. No	Parameters	Enhancement of Heat Transfer Coefficient	Factor to Be Analyzed	Reference
1	Multiple Fins Introduction	4.2%	Multiple fins geometries	[31]
2	Flow Patterns of Staggered and Inline Shape Heat Exchanger	5.4%	Staggered and inline flow patterns	[18]
3	Shell Side Analysis	9.4%	Shell side examination of the heat exchanger	[32]
4	Round and Hexagonal Tubes	13.46%	Round and hexagonal tubes	Current Study

4. Conclusions

In this research work, we performed computational fluid dynamics (CFD) simulations and experimental analysis on the shell and tube heat exchangers using round and hexagonal tubes for a range of flow velocities using both parallel flow and counter flow arrangements. The examination is carried out with the fluid velocity ranging from 0.75 m/s to 2.75 m/s at the Reynolds number of 10,000 to 15,000. The following are some major conclusions drawn from the study.

The rate of heat transfer is directly proportional to the number of turns of the tube and the velocity of the floating fluid. The velocity of the fluid determines the proportion of the eddies. As a result, molecular dispersion is increased by enlarging the fluid velocity. The optimum velocity where the maximum heat transfer is accomplished is 2.75 m/s.

Hexagonal geometry increases the surface for heat transfer that enhances the proportion of the molecules conducting heat. As a result, the efficiency of the heat exchanger is increased.

By introducing the hexagonal tubes, the heat transfer rate and contact surface area signify up to 13.5% and 31.8%, respectively.

Hexagonal tubes increase the pressure drop of a fluid by increasing the steady volume that maximizes the density difference in a loop that acts as a driving force for heat to transfer between the shell and the tube fluids.

By increasing the number of the turns of the tube, the turbulence to the boundary layer is increased.

The uncertainty in round tubes (9.2%) is greater than in hexagonal tubes (4.2%) because the blockage effect becomes sounder in the circular round geometry of tubes.

This research has some future commendations that are determined below.

In the future, the effect of the hexagonal tubes can be analyzed by introducing different environmental conditions in the shell and the tube of a heat exchanger.

Experimental and numerical investigation of heat exchanger tubes can be performed with the optimization of its shape, so that it has a significant surface area that increases the heat transfer rate.

Supplementary Materials: The following supporting information can be downloaded at: https://www.mdpi.com/article/10.3390/en16020880/s1, Figure S1: End capes and Shell of heat exchanger; Figure S2: Projected Surface area; Figure S3: Cross section meshes; Figures S4 and S5: multiple experimental components; Figure S6: Assembling operations of the tubes; Table S1: Experimental apparatus details; Videos S1–S3: Various manufacturing operations.

Author Contributions: Conceptualization, A.K. and I.S.; methodology A.K., W.G. and T.A.K.; software, Y.A., W.G. and T.A.K.; writing—original draft preparation, A.K., W.G. and I.S.; writing—review and editing, S.A.M., A.K., I.S., T.A.K., Y.A. and W.G.; supervision, I.S. and W.G.; project administration, S.A.M. and Y.A.; funding acquisition, I.S. All authors have read and agreed to the published version of the manuscript.

Funding: This research received no external funding.

Data Availability Statement: Data is available in the attached supplementary file.

Conflicts of Interest: The authors declare no conflict of interest.

Nomenclature

Symbol	Meaning
U	Overall Heat Transfer Coefficient
Q°	Heat Transfer Rate
ΔT_{lm}	Logarithmic Mean Temperature
T_{hi}	Hot inlet temperature
T_{ho}	Hot outlet temperature
T_{ci}	Cold inlet temperature
T_{co}	Cold outlet temperature
∇	Del Operator
Φ	Phi (irrational mathematical constant, approximately 1.618)
u	Viscosity
∂	Partial
λ	Wavelength

References

1. McClintock, F.A. The design of heat exchangers for minimum irreversibility. *ASME Paper* **1951**, *51*, 108. [CrossRef]
2. Caputo, A.C.; Pelagagge, P.M.; Salini, P. Heat exchanger design based on economic optimisation. *Appl. Therm. Eng.* **2008**, *28*, 1151–1159. [CrossRef]
3. Fernandes, E.J.; Krishanmurthy, S.H. Design and analysis of shell and tube heat exchanger. *Int. J. Simul. Multidiscip. Des. Optim.* **2022**, *13*, 15. [CrossRef]
4. Xu, X.; Zhang, X.; Ke, P.; Wang, C.; Yang, H.; Yang, C. Study on the heat transfer characteristic of compact heat exchanger based on experimental data. *Procedia Eng.* **2015**, *121*, 293–299. [CrossRef]
5. Henry, M.; Mercado, R. Advances in Coriolis mass flow metering research and technology. *Atp Int.* **2005**, *3*, 24–32.
6. Johnson, J.; Shani, A. CFD analysis of double pipe heat exchanger. *Int. J. Sci. Eng. Technol. Res.* **2015**, *4*, 1283–1286.
7. Fakheri, A. Heat Exchanger Efficiency. *J. Heat Transf.* **2006**, *129*, 1268–1276. [CrossRef]
8. Gholizadeh, A.; Pourfallah, M.; Gholinia, M.; Armin, M.; Languri, E. The role of nanofluids and fins in a heat exchanger on waste energy recovery from a diesel engine: An experimental and numerical study. *Energy Rep.* **2022**, *8*, 13353–13368. [CrossRef]
9. Jaya Chandran, T.R.V. Analysis of fin and tube heat exchanger for liquid to liquid heat transfer applications. *Int. J. Eng. Res. Technol.* **2014**, *3*, 359–362. Available online: www.ijert.org (accessed on 1 March 2019).
10. Ravikumar, K.; Raju, C.N.; Saheb, M. CFD Analysis of a cross-flow heat exchanger with different fin thickness. *Int. J. Dyn. Fluids* **2017**, *13*, 345–362.
11. Pelikán, M.; Gášpár, R. CFD analysis of water cooling heat exchanger for storage energy from exhaust pipe. *AIP Conf. Proc.* **2018**, *2047*, 020017. [CrossRef]
12. Perone, C.; Romaniello, R.; Leone, A.; Catalano, P.; Tamborrino, A. CFD analysis of a tubular heat exchanger for the conditioning of olive paste. *Appl. Sci.* **2021**, *11*, 1858. [CrossRef]
13. Kalvig, S.; Manger, E. Comparing different CFD wind turbine modelling approaches with wind tunnel measurements Comparing different CFD wind turbine modelling approaches with wind tunnel measurements. *Conf. Ser.* **2014**, *555*, 012056. [CrossRef]
14. Li, Q.; Jia, H.; Qiu, Q.; Lu, Y.; Zhang, J.; Mao, J.; Fan, W.; Huang, M. Typhoon-Induced Fragility Analysis of Transmission Tower in Ningbo Area Considering the Effect of Long-Term Corrosion. *Appl. Sci.* **2022**, *12*, 4774. [CrossRef]

15. Singh, G.; Kumar, H. Computational fluid dynamics analysis of shell and tube heat exchanger. *J. Civ. Eng. Environ. Technol.* **2014**, *1*, 66–70.
16. Babu, C.R.; Gugulothu, S.K. CFD analysis of heat transfer enhancement by using passive technique in heat exchanger. *Int. J. Recent Adv. Mech. Eng.* **2015**, *4*, 99–111. [CrossRef]
17. Kishan, R.; Singh, D.; Sharma, A.K. CFD Analysis of heat exchanger models design using ansys fluent. *Int. J. Mech. Eng. Technol.* **2020**, *11*, 1–9. [CrossRef]
18. Sharma, S.; Sharma, S.; Singh, M.; Singh, P.; Singh, R.; Maharana, S.; Khalilpoor, N.; Issakhov, A. Computational fluid dynamics analysis of flow patterns, pressure drop, and heat transfer coefficient in staggered and inline shell-tube heat exchangers. *Math. Probl. Eng.* **2021**, *2021*, 6645128. [CrossRef]
19. Kumar, P.M.; Chandrasekar, M. CFD analysis on heat and flow characteristics of double helically coiled tube heat exchanger handling MWCNT/water nanofluids. *Heliyon* **2019**, *5*, e02030. [CrossRef]
20. Singh, N.; Ali, R. CFD Analysis of condensation heat transfer in helical coil heat exchanger. *SSRN Electron. J.* **2019**, *3*, 1–8. [CrossRef]
21. Mickan, B.; Strunck, V. A primary standard for the volume flow rate of natural gas under high pressure based on laser Doppler velocimetry. *Metrologia* **2014**, *51*, 459–475. [CrossRef]
22. Paper, C.; Uruba, V. On reynolds number physical interpretation. *AIP Conf. Proc.* **2018**, *2000*, 020019. [CrossRef]
23. Shah, I.; Jeon, H.S.; Ali, M.; Yang, D.H.; Choi, K.-H. Optimal parametric mixing analysis of active and passive micromixers using Taguchi method. *Proc. Inst. Mech. Eng. Part E J. Process Mech. Eng.* **2019**, *233*, 1292–1303. [CrossRef]
24. Aziz, S.; Khan, A.; Shah, I.; Khan, T.A.; Ali, Y.; Sohail, M.U.; Rashid, B.; Jung, D.W. Computational fluid dynamics and experimental analysis of a wind turbine blade's frontal section with and without arrays of dimpled structures. *Energies* **2022**, *15*, 7108. [CrossRef]
25. Ikumapayi, O.M.; Akinlabi, E.T.; Madushele, N.; Fatoba, S.O. A brief overview of bending operation in sheet metal forming. *Lect. Notes Mech. Eng.* **2020**, *6*, 149–159. [CrossRef]
26. Noura, Z.; Shah, I.; Aziz, S.; Ahmed, A.; Jung, D.-W.; Brahim, L.; ElMostafa, R. Wearable healthcare monitoring based on a microfluidic electrochemical integrated device for sensing glucose in natural sweat. *Sensors* **2022**, *22*, 8971. [CrossRef]
27. Utamura, M.; Nikitin, K.; Kato, Y. Generalization of logarithmic mean temperature difference method for heat exchanger performance analysis. *Therm. Sci. Eng.* **2008**, *15*, 163–173.
28. Cui, X.; Chua, K.J.; Islam, M.R.; Yang, W.M. Fundamental formulation of a modified LMTD method to study indirect evaporative heat exchangers. *Energy Convers. Manag.* **2014**, *88*, 372–381. [CrossRef]
29. Doering, C.R.; Gibbon, J.D. *Applied Analysis of the Navier-Stokes Equations, No. 12*; Cambridge University Press: Cambridge, UK, 1995.
30. Temam, R. *Navier-Stokes Equations: Theory and Numerical Analysis*; American Mathematical Society: Providence, RI, USA, 2001; Volume 343.
31. Basavarajappa, S.; Manavendra, G.; Prakash, S.B. A review on performance study of finned tube heat exchanger. *J. Phys. Conf. Ser.* **2020**, *1473*, 12030. [CrossRef]
32. Petrik, M.; Szepesi, G.L. Shell side CFD analysis of a model shell-and-tube heat exchanger. *Chem. Eng. Trans.* **2018**, *70*, 313–318. [CrossRef]